ADVANCED THERAPEUTICS
www.advtherap.com

Core-Shell Functionalized Zirconium-Pemetrexed Coordination Nanoparticles as Carriers with a High Drug Content

*Benjamin Steinborn, Patrick Hirschle, Miriam Höhn, Tobias Bauer, Matthias Barz, Stefan Wuttke, Ernst Wagner, and Ulrich Lächelt**

Selected drug molecules with Lewis base functions can be assembled into coordinative nanoparticles (NPs) by linking them with suitable metal ions. Such nanomaterials exhibit a high material economy due to high drug contents and minor amounts of inactive additives. The antifolate pemetrexed (PMX) which is used for the treatment of lung cancers contains two carboxy functions that are able to undergo coordinative binding of metal ions. This study presents the development of a multilayer PMX NP system where each layer serves a distinct purpose. The metal-drug NP core is assembled in a bottom-up approach by coordinative interactions between zirconium (IV) ions and PMX molecules. Since the NP core is generated from drug molecules as essential units, it features a very high drug content of almost 80%. The NP core is stabilized against serum with a shell of a polymerized oligoamine-modified trimethoxysilane derivative (TMSP). As external layer, a polyglutamate-*block*-polysarcosine-N_3 (pGlu-*b*-pSar) coating mediates efficient colloidal stabilization and enables introduction of targeting functionalities by click chemistry. Attaching folate or transferrin ligands to the polymer layer enhances NP uptake into target receptor positive KB and L1210 cells. This study illustrates the development and characterization of metal-drug coordination NPs with high drug content and variable external functionalizations.

1. Introduction

Pharmacokinetic properties are inherent characteristics of drug molecules that cannot be changed without derivatization. Nanoparticles (NPs) which are small enough to circulate in the bloodstream and carry cargo molecules are attractive materials for the utilization as drug containers since their pharmacokinetic properties can be tuned without affecting the pharmacodynamics of the drug. NP drug delivery systems are therefore being investigated to overcome the poor selectivity and major side effects frequently associated with chemotherapy.[1] Conventional chemotherapy often suffers from unfavorable pharmacokinetics, limited tumor accumulation, and systemic toxicity. As a consequence, high doses are required for efficient tumor treatment but the severe dose-limiting off-target effects determine a narrow therapeutic window and impair patient benefits in the clinical practice.[2] Recent approaches in nanotechnology work toward ameliorating the situation by developing chemotherapeutic NP formulations aimed at increasing drug selectivity toward neoplastic tissues by employing active and passive targeting strategies of single or combination therapies[3] and enhancing therapeutic indices.[4] At present, about 40 nanomedicines,[5] for instance liposomal doxorubicin[6] and iron-oxide NP formulations,[7] are used for a variety of indications. Recently, highly regular coordination polymers such as metal-organic frameworks[8] (MOFs) have emerged as an additional class of nanomaterials.[9] Several MOFs utilize polydentate carboxylic acid linkers and their

B. Steinborn, M. Höhn, Prof. E. Wagner, Dr. U. Lächelt
Department of Pharmacy and Center for NanoScience (CeNS)
LMU Munich
81377 Munich, Germany
E-mail: ulrich.laechelt@cup.uni-muenchen.de

The ORCID identification number(s) for the author(s) of this article can be found under https://doi.org/10.1002/adtp.201900120

DOI: 10.1002/adtp.201900120

P. Hirschle, Prof. S. Wuttke
Department of Chemistry and Center for NanoScience (CeNS)
LMU Munich
81377 Munich, Germany

T. Bauer, Dr. M. Barz
Institute of Organic Chemistry
Johannes Gutenberg-University Mainz
55099 Mainz, Germany

T. Bauer
Max Planck Graduate Center
55128 Mainz, Germany

Prof. S. Wuttke
BC Materials
Basque Center for Materials
UPV/EHU Science Park 48940 Leioa, Spain

coordinative interactions with metal ions to obtain defined crystalline structures. As MOFs span a rich chemical space of about 70 000 reported structures[10] with varying degrees of porosity[8b,11] and tailorable sizes,[12] they are mainly explored for catalysis,[13] gas storage,[14] separation,[15] sensing,[16] and drug delivery[3,17] applications. However, delivering small molecule drugs by encapsulation into MOF pores is not trivial and depending on the used drug and MOF, the drug content varies significantly.[17g] High drug loading is generally a desired parameter of drug delivery systems in order to minimize exposure of patients to nanocarrier material and reduce possible adverse reactions. Moreover, the aim of a high drug to carrier ratio corresponds to the modern concepts of "atom economy" and "multifunctional efficiency" in the context of NPs.[18] Hypothetical nanopharmaceuticals with the highest imaginable drug to carrier ratio and most simple synthesis would be composed of drug molecules only which assemble into NPs themselves. On the other hand, conventional therapeutic agents mediate their pharmacological effect in a dissolved state and a dynamic conversion from stable drug colloids to solubilized drug molecules is required. In general, native drug molecules do not fulfill these requirements. Approximations of these envisioned ideal nanopharmaceuticals are represented by metal-drug NPs. By replacing the pharmacologically inactive linkers typically used to synthesize MOFs with polydentate carboxy-containing or phosphate-modified active pharmaceutical ingredients, for instance, disuccinatocisplatin,[19] acetaminophen phosphate,[20] or methotrexate,[21] coordination polymers with higher drug contents and multifunctional efficiencies are feasible. However, in many cases such structures seem to exhibit limited physiological stabilities and require further stabilizing surface modifications as observed and addressed by Rieter et al.[19b] and Huxford et al.[21]

Here, we report the development of a novel hybrid coordinative NP (Zr-PMX NP) based on zirconium ions (Zr^{4+}) and pemetrexed (PMX), an antifolate drug used for lung cancer pharmacotherapy.[22] The aim of the study was the generation of metal-drug nanopharmaceuticals with a high drug loading capacity, favorable colloidal stability, the possibility for modification with receptor ligands and preserved pharmacological activity of the drug. The Zr-PMX core with a very high drug content was sequentially modified with silica and polymer shells in order to achieve suitable serum and colloidal stabilities and allow for the introduction of targeting ligands. The presented strategy for the assembly of a multifunctional nanopharmaceutical with a very high drug content is considered to be a versatile platform translatable to other drug molecules with functional groups capable of coordinative interaction with metal ions.

2. Results

2.1. Development and Characterization of the Zr-PMX NP Core

Scheme 1 provides an overview of the sequential assembly of multifunctional Zr-PMX NPs. First, the drug-containing NP core is generated using the synthetic parameters described in Scheme 1A. Scheme 1B depicts the addition of a silica layer to enhance the NP core stability. The external silica surface is finally coated with a polyglutamate-*block*-polysarcosine block copolymer for simultaneous colloidal stabilization, sterical shielding, and attachment of targeting ligands as illustrated in Scheme 1C. Dynamic light scattering (DLS) measurements of the final formulations confirming the assembly of NPs are depicted in Figure S1, Supporting Information. Zirconium(IV) was chosen as the metal component for the assembly of the drug containing NP core due to its ability to form stable metal-organic complexes with suitable biological tolerability as observed before with other Zr-based MOFs and drug delivery systems.[23] The particles were formed at room temperature within 45 min in an ethanol-water mixture containing HCl and 100 equivalent formic acid as additives for control of particle growth. The optimal linker:metal ratio varies upon different Zr-based metal-organic nanomaterials, such as 1:1[24] or 3:1,[20,25] therefore a range of PMX to Zr stoichiometries was initially screened in this study. A molar excess of PMX is favorable in terms of lower polydispersity indices (PDIs), as observed for 3:1 and 3:2 ratios compared to equimolar 3:3 (Figure S2, Supporting Information) with *z*-averages between 130 and 220 nm. In case of excessive Zr at a 3:6 ratio, only minor particle formation could be observed within the 45 min reaction time (Figure S1, Supporting Information). A possible explanation lies within a higher number of initially formed crystal nuclei which results in the NP growth being distributed over more individual particles leading to slower growth of single particles as described by Wang et al.[26] Satisfactory PDI and particle yield were achieved at a 3:1 PMX to Zr ratio and these conditions were used for subsequent studies. In order to generate particles within the nanometer size range suitable for biological applications,[27] acid was added to the reaction mixture. For samples without any acidification, rapid clouding and formation of particles in the micrometer range were observed. By adding 100 equivalents formic acid, a monodentate modulator also used for MOF synthesis,[24b,28] this immediate aggregation was prevented and the particle formation occurred more slowly (Figure S3, Supporting Information). Additional HCl had a minor influence on size and PDI (Figure S4, Supporting Information). Sonication of the obtained NPs mediated favorable effects on the particle size by disaggregating agglomerates formed during the centrifugation and washing steps (Figure S5, Supporting Information). The overall effect of sonication was about 100 nm of size decrease and 5 min of sonication was determined to be sufficient, longer durations did not mediate a further improvement. We found that the fluorescent dye calcein, which contains several Lewis base functions and forms chelates with metal ions, can be co-assembled into the NP core. Notably, the addition of 5% calcein only had a minor influence on *z*-average and PDI (Figure S6, Supporting Information) and enables fluorescence-based detection by confocal microscopy or flow cytometry studies without the requirement for additional labeling. Moreover, this illustrates the flexibility of the presented particle assembly concept and the possibility to encapsulate different cargos. We further investigated the NP core (Scheme 1A) with regard to its physicochemical properties (**Figure 1**). Analysis by scanning-electron microscopy (SEM, Figure 1A) revealed a particle diameter of 64.26 ± 10.09 nm ($n = 100$).

The difference in size compared to the previously presented DLS data can be attributed to the individual techniques, SEM-imaging measures particles in dry form whereas DLS determines their hydrodynamic diameter in solution.[29] Energy dispersive

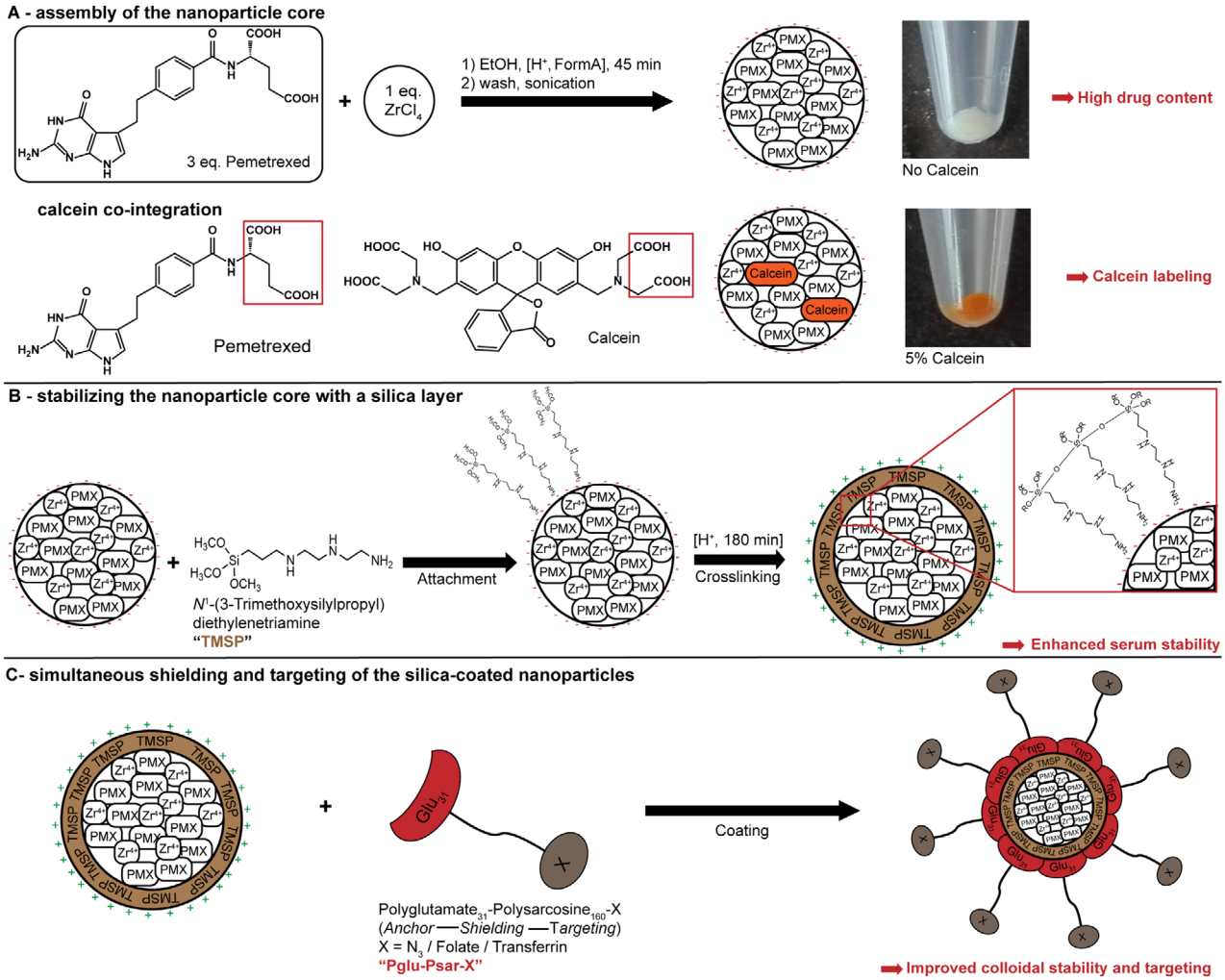

Scheme 1. Overview of the utilized core-shell nanoparticle (NP) assembly approach. A) Synthesis of the drug-containing NP core and labeling by coordinative integration of fluorescent calcein dye; B) stabilization of the NP core by a polymerized silica shell; and C) simultaneous shielding and targeting by coating with polyglutamate-polysarcosine block copolymers.

X-ray spectroscopy (Figure 1B) confirmed the presence of key elements, oxygen and carbon as part of the PMX structure and zirconium as well as chloride due to the used metal compound and the added HCl. The carbon signal can also be partially attributed to the conductive carbon layer added during SEM sample preparation. X-ray diffraction (XRD) (Figure 1C) did not show crystallinity, which is why we assume an amorphous structure of Zr-PMX NPs. The porosity and surface area of the dried NPs were investigated using nitrogen sorption (Figure 1D). Evaluating the sorption isotherms with the BET method,[30] resulted in a surface area of 170 $m^2\ g^{-1}$, suggesting porosity in the sample. Both the nitrogen sorption isotherm and the corresponding pore size distribution indicate this porosity stems mainly from mesopores starting at 40 Å. Next, the PMX to Zr mass ratio present in the NP core was determined (Figure 1E) by inductively coupled plasma atom emission spectrometry (ICP-AES) and high-performance liquid chromatography (HPLC). ICP-AES revealed a Zr content of 20.03 ± 0.96% (m/m, $n = 3$). NP lysis followed by PMX quantification by HPLC showed a PMX content of 78.23 ± 1.83% (m/m, $n = 3$). Similarly high drug contents have been observed by Heck et al. for other zirconium-based drug formulations.[20,31] Considering the Zr(IV) coordination number of six and two coordinatively active carboxy functions per PMX molecule, our obtained result is close to the hypothetical PMX to Zr ratio of 3 and also corresponds to the feed ratio during NP synthesis. For Zr-PMX NP, thermogravimetric analysis indicated a residual particle mass of 33.85% (Figure 1F). As the NP sample was heated in a mixed N_2/O_2 atmosphere, which led to the formation of ZrO_2, the actual metal content is lower. By excluding the oxide formation (MW $ZrO_2 = 123.22\ g\ mol^{-1}$, MW $Zr = 91.22\ g\ mol^{-1}$, factor: 1.35), the amount of non-oxidized Zr present in the NP can be estimated as 33.85%/1.35 = 25.05%, which differs only slightly from the result determined by ICP–AES and also agrees very well with the hypothetical particle composition. Next, the long-term stability of as-synthesized NPs (Figure 1G) was evaluated in ethanol (EtOH) at room temperature by performing DLS measurements every 24 h. After 48 h, a minor increase in *z*-average was observed whereas the PDI remained unchanged over 96 h. As a precaution, the freshly prepared NPs were thus stored for a maximum of 24 h for all experiments.

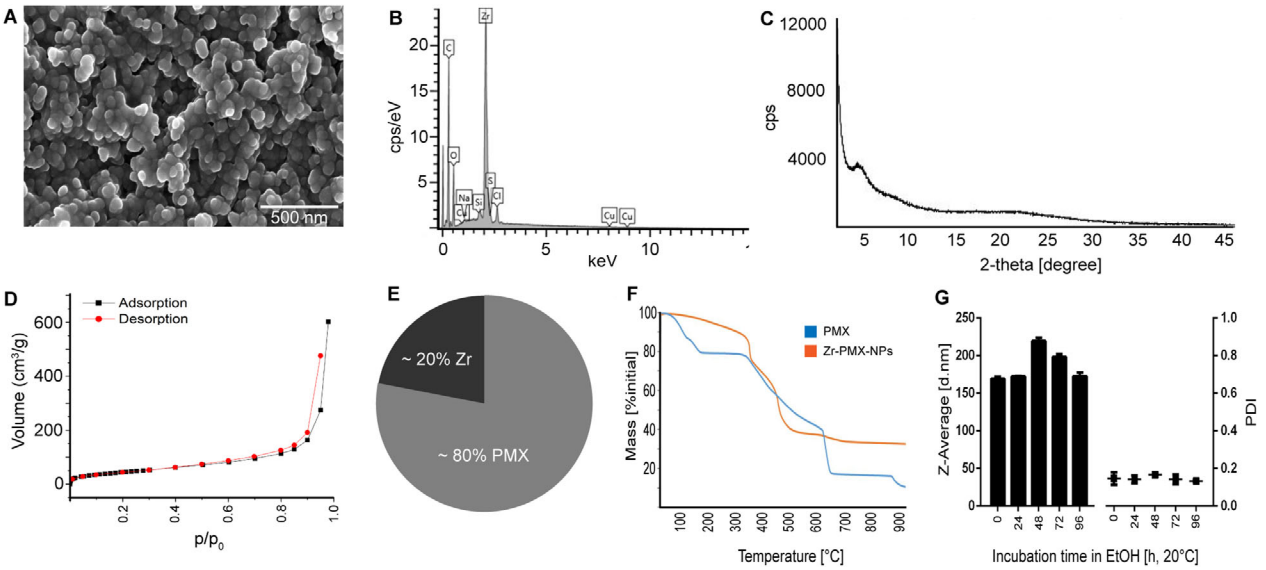

Figure 1. Physiochemical characterization of the NP core containing the drug payload. A) Imaging by scanning-electron microscopy; B) qualitative elemental composition determined by energy dispersive X-ray spectroscopy; C) analysis of crystallinity by X-ray diffraction; D) measurement of porosity by nitrogen sorption analysis; E) particle composition by ICP–AES and HPLC (mean, $n = 3$); F) thermogravimetric analysis; and G) particle size, polydispersity and stability in ethanol by dynamic light scattering (mean ± SD, $n = 3$).

2.2. Silica coating of Zr-PMX NP Cores Enhances their Serum Stability and Uptake into Cancer Cells

Initial exploratory serum stability studies of the as-synthesized Zr-PMX NP core revealed a high PMX release within 30 min of serum incubation. In order to increase and control the stability, we developed and applied a silica coating strategy to the nanosystem. Although tetraethylorthosilicate (TEOS) is commonly used for silica coatings,[32] this study utilized N^1-(3-trimethoxysilylpropyl)diethylenetriamine (TMSP) instead, which has, to the best of our knowledge, only been previously employed as a silica coating agent in a physicochemical setting[33] but not for a biological or drug delivery application. Coating NPs with a silica shell based on TEOS by applying the Stöber method[34] typically requires an interfacing step by attaching a polymer, such as poly-(vinylpyrrolidone) (PVP), to the NP surface in order to maintain colloidal NP stability under the conditions of the Stöber process.[32b,35] However, such a step introduces additional complexity to the system and the used type of PVP determines the final particle characteristics.[35] Liz-Marzán et al. directly coated gold NPs using (3-aminopropyl)trimethoxysilane as the interfacing agent before applying the Stöber method to deposit an additional TEOS layer.[36] This inspired us to use TMSP which we perceived as even more suitable compared to (3-aminopropyl)trimethoxysilane due to its diethylenetriamine motif providing additional interaction sites for coordinative and/or electrostatic attachment to the surface of Zr-PMX NPs (Scheme 1B). As shown in **Figure 2**, we screened the influence of the used TMSP amount and coating duration by DLS (Figure 2A) and then proceeded to further characterize the obtained Zr-PMX@TMSP NPs by SEM, energy dispersive x-ray spectroscopy (EDX), and XRD.

Interestingly, coating times up to 5 h with the highest tested TMSP amount of 3 µL resulted in small NPs and similar PDI values whereas 24 h of coating with TMSP amounts of 1.5 µL or higher resulted in strong particle aggregation and increased polydispersity. The coating process mediated a distinct zeta potential inversion from -20.8 ± 0.6 mV to 25.9 ± 1.1 mV or higher, which did not change further after 5 h of coating time. After performing an aqueous wash to remove silica polymerization by-products (Figure S7, Supporting Information), SEM-imaging (Figure 2B) indicated a silica-coated NP size of 74.57 ± 16.64 nm ($n = 100$), which implies an increase in diameter of approximately 10 nm compared to the uncoated NP core and, thus, a silica shell thickness of about 5 nm. Besides the increase in size and the observed zeta potential inversion, EDX analysis (Figure 2C) also confirmed the presence of a silica peak. XRD analysis (Figure 2D) revealed an additional peak at a 2-θ of approximately 25° which can be attributed to polymerized TMSP; a control spectrum of polymerized TMSP without NPs (Figure S8, Supporting Information) confirms this suggestion. Next, the effects of the silica coating on the serum stability were evaluated in a time- and dose-dependent manner (**Figure 3**). Here, a distinct effect of the TMSP amount on the PMX release in serum (Figure 3A) was observed.

After 30 min of incubation in 10% fetal bovine serum (FBS), approximately 70% of the incorporated PMX was released from the uncoated NPs. Coating with 1.5 µL TMSP reduced the release to approximately 50% independent of the coating duration. The stabilizing effect was further increased with 3 µL TMSP. Here, the observed PMX release was reduced to approximately 25%. In all cases, the coating duration had a minor effect on the serum stability. We hypothesize that the TMSP layer stabilizes the NP core by impairing the interaction between PMX and serum protein. PMX is known to exhibit a high degree of protein binding[37] which might compete with the coordinative zirconium interactions that mediate formation of the NP core. Higher amounts of TMSP are likely to further enhance the

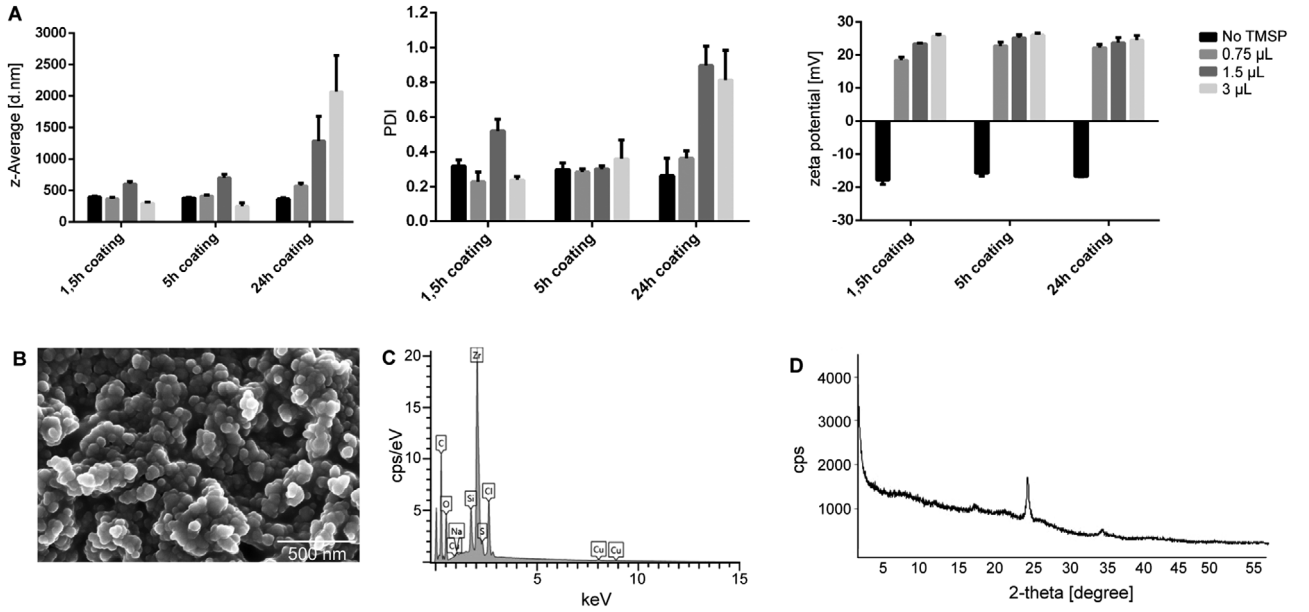

Figure 2. Characterization of the silica coating. A) Effects of TMSP amount and coating duration on particle size determined by dynamic light scattering (mean ± SD, n = 3); B) imaging of the silica-coated NPs by scanning-electron microscopy; C) qualitative elemental analysis by energy dispersive X-ray spectroscopy and D) evaluation of crystallinity by X-ray diffraction.

stability. However, since the drug mediates its activity in a solubilized state and has to be released from the nanocolloids, we considered the achieved TMSP effect to represent a suitable balance between required stability and lability. Next, the effect of the TMSP-coating on the uptake of calcein-containing Zr-PMX NP cores was evaluated on adherent A549 (human lung adenocarcinoma, Figure 3B) and L1210 (mouse lymphocytic leukemia Figure 3C) suspension cell lines using confocal laser scanning microscopy (CLSM). For both cell lines, the coating increased the overall NP uptake, likely due to the increased serum stability and the zeta inversion resulting in enhanced unspecific electrostatic uptake as described for other nanosystems.[38] This observation was additionally confirmed using human cervix carcinoma KB cells and quantified by flow cytometry (Figure S9, Supporting Information). TMSP-coated Zr-PMX NPs mediated significantly higher median calcein fluorescence compared to uncoated NPs or free calcein. The CLSM studies however revealed an external NP attachment to the cell membrane and extracellular aggregation, which illustrated the need for further colloidal stabilization in a biological environment. Since increased colloidal stability of Zr-based MOFs has been achieved with a polyglutamate-*block*-polysarcosine copolymer before,[39] we intended to adapt this strategy to Zr-PMX@TMSP NPs.

2.3. Coating Zr-PMX@TMSP NPs with pGlu-*b*-pSar Mediates Efficient Shielding

In order to enhance the colloidal stability of Zr-PMX@TMSP NPs, a sterical shielding was implemented by surface coating with a polyglutamate$_{31}$-polysarcosine$_{160}$-N_3 (pGlu-*b*-pSar) block copolymer.[40] It has been shown in previous studies with Zr-*fum* NPs that the polyglutamate block serves as the NP binding and surface attachment module while the polysarcosine block mediates efficient shielding, colloidal stabilization, and prevention of protein interactions.[39,41] Additionally, Finsinger et al. reported steric stabilization and reduced complement activation for a cationic nanostructure coated with an anionic PEG-derived copolymer.[42] In order to stabilize our Zr-PMX@TMSP NPs, an initial dose titration experiment was carried out by mixing equal amounts of Zr-PMX@TMSP NPs with different amounts of pGlu-*b*-pSar (**Figure 4**).

Adding 500 µL of NP in HEPES-buffered glucose (HBG) to up to 50 µg of polymer did not notably influence its *z*-average and PDI but a zeta potential reduction depending on the polymer dose was observed (Figure 4B). Zr-PMX@TMSP NPs without pGlu-*b*-pSar coating exhibited a zeta potential of 28.73 ± 1.55 mV, which was reduced to 1.19 ± 0.06 mV by addition of 25 µg pGlu-*b*-pSar. Increasing the amount of offered polymer did not result in a further zeta potential reduction, we therefore concluded that 25 µg pGlu-*b*-pSar was sufficient to induce the observed zeta potential shift toward neutrality, which is known to benefit NPs by reducing unspecific uptake, immune recognition, and prolonging circulation half-lives.[38a,43] Next, we investigated how the pGlu-*b*-pSar coating influenced the colloidal NP stability at 37 °C. Incubating uncoated Zr-PMX@TMSP NPs in HBG (Figure 4C) led to increasing aggregation over time; after 96 h the *z*-average almost doubled and a slight increase in PDI was observed. In contrast, the pGlu-*b*-pSar-coated NPs did not increase in size, retained their neutral zeta potential and showed no difference in PDI over 96 h. The colloidal stability was also evaluated in phosphate-buffered saline (PBS, Figure 4D) which is a relevant biological buffer and challenging due to the strong

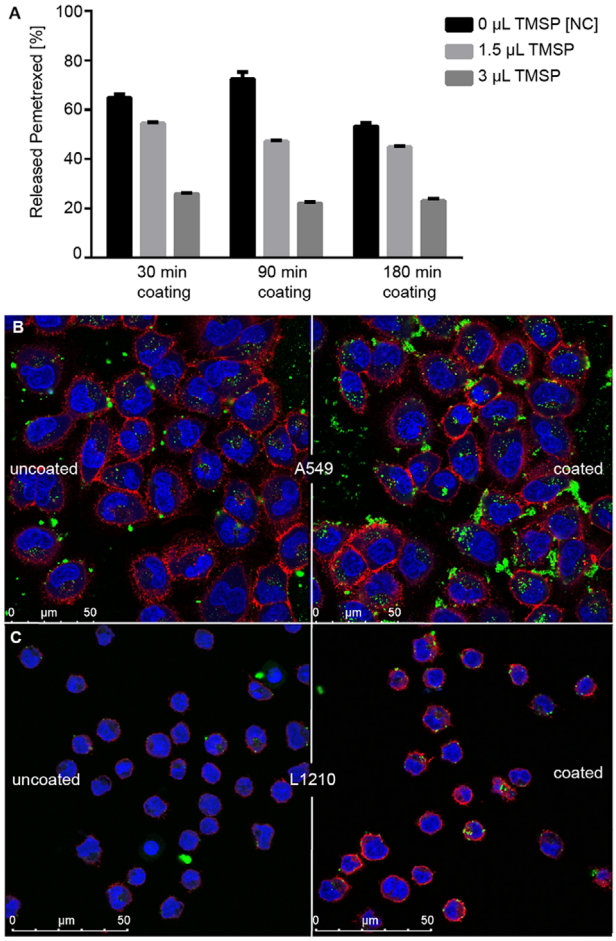

Figure 3. The silica coating enhances the serum stability and promotes NP uptake into cancer cells. A) Serum stability of TMSP-coated NPs determined by HPLC (mean ± SD, $n = 3$); B) effects of the coating on NP uptake into adherent A549 lung adenocarcinoma or (C) suspension L1210 leukemia cells visualized by CLSM. Green, NP core labeled by coordinative integration of calcein; Red, actin stained with phalloidin-rhodamine; Blue, nuclei stained with DAPI.

interaction between phosphate and zirconium ions.[20,31,44] Indeed, the uncoated NPs immediately aggregated to agglomerates in the micrometer range and the sizes further increased over time. In contrast, no increase in size or PDI was observed for the pGlu-*b*-pSar coated Zr-PMX@TMSP NPs during 96 h of incubation in PBS which illustrated the enormous colloidal stabilization induced by the polymer coating. We also investigated if the polymer remained attached to the NP surface under serum-containing cell culture conditions (Figure 4E) since one could expect competition between the polymer and negatively charged serum protein for binding to the positively charged silica shell. The azide-containing pGlu-*b*-pSar block copolymer was therefore labeled with DBCO-Alexafluor647 via strain-promoted alkyne-azide cycloaddition (SPAAC). We then proceeded to incubate calcein-containing Zr-PMX@TMSP NPs coated with pGlu-*b*-pSar-AF647 on KB cells. After a total of 4 h incubation, confocal microscopy showed yellow signals in the merge channel which indicated co-localization between the calcein integrated into the NP core (green channel) and the AF647-labeled polymer shell (red channel). Examination of co-localization using the Manders coefficient[55] revealed values of $M1 = 0.996$ and $M2 = 0.684$ (channel 1: pGlu-*b*-pSar-AF647, channel 2: calcein). Based on those findings, the polymer seems almost quantitatively co-localized (~99.6%) with the calcein signal (NP core) as illustrated by Manders M1. Manders M2 reveals that approximately 68.4% of the calcein signal are co-localized with the polymer. We therefore concluded that the polymer remained attached to the NP surface under serum conditions, especially since almost no isolated red signal representing detached polymer was observed in the merge channel.

2.4. Attachment of Targeting Ligands to the Polymer Shell Enhances the NP Uptake

In order to improve NP uptake and selectivity toward cancer cells, we introduced folate targeting, a concept initially developed by Leamon and Low,[45] to our nanosystem. The folate receptor is known to be overexpressed for many cancer types[46] and the low dissociation constant (K_d approximately 0.1 nM for the α-isoform),[47] makes folate an attractive ligand for selective cancer targeting.[48] A folate-modified block copolymer (pGlu-*b*-pSar-FolA) was synthesized by coupling the azide-containing pGlu-*b*-pSar to a DBCO-folic acid (DBCO-FolA)[49] building block via SPAAC. Coating Zr-PMX@TMSP NPs with pGlu-*b*-pSar-FolA (Figure S10, Supporting Information) as shown in **Figure 5** led to a nanoformulation with folic acid attached to the polysarcosine terminus. Based on the polymer dose titration experiment shown in Figure 4, which identified 25 µg of polymer as sufficient for surface saturation of the used amount of NPs, we initially evaluated by DLS how modifying Zr-PMX@TMSP NPs with 25 µg pGlu-*b*-pSar containing different ratios of pGlu-*b*-pSar-FolA influenced NP size, PDI, and zeta potential (Figure 5A). Compared to 0% pGlu-*b*-pSar-FolA, a content of up to 75% pGlu-*b*-pSar-FolA did not notably influence any of these parameters. Coating with 100% pGlu-*b*-pSar-FolA led to aggregation, presumably as a result of the high content of hydrophobic ligands and the decreased electrostatic repulsion.[50]

After confirming folate receptor expression by flow cytometry (Figure S11, Supporting Information), the effect of folate on NP uptake was tested by confocal microscopy using adherent KB (human cervix carcinoma, Figure 5C) and suspension L1210 (mouse lymphocytic leukemia, Figure 5D) cell lines. On both cell lines, an enhanced uptake was observed for the folate-containing nanopharmaceuticals compared to the untargeted formulation. Flow cytometry analysis on KB cells (Figure 5B) provided additional confirmation of the increased uptake of folate-targeted NPs compared to an untargeted control formulation coated with pGlu-*b*-pSar only. A control sample with an equal concentration of free calcein was also analyzed and did not show any uptake. Importantly, this provided additional evidence that the presented coordination NPs can mediate cellular uptake of cargos that do not cross the cell membrane on their own. We also developed a transferrin-functionalized formulation presented in **Figure 6** since the transferrin receptor is frequently

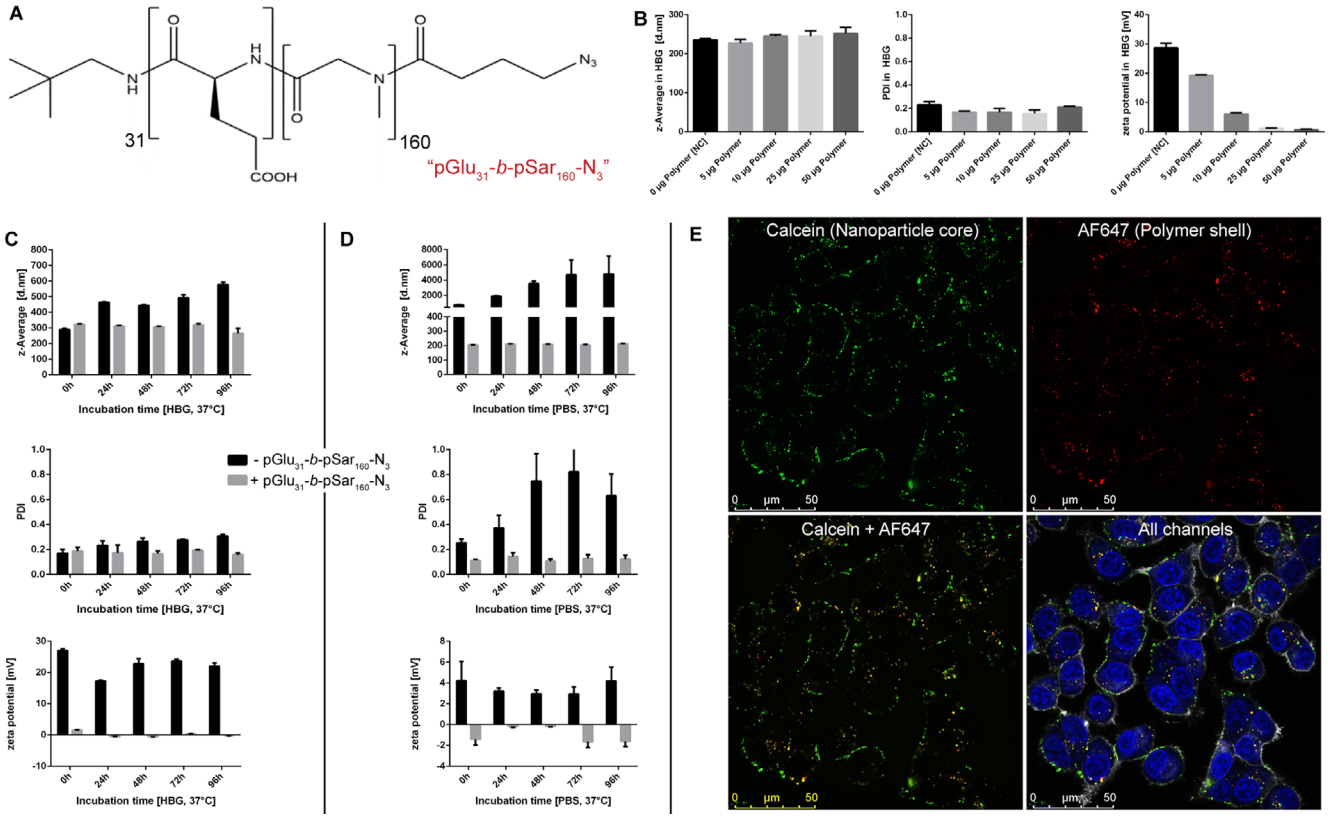

Figure 4. Characterization of the pGlu-pSar coating. A) Structure of $pGlu_{31}$-*b*-$pSar_{160}$-N_3; B) polymer dose titration and the influence on size, PDI, and zeta potential by DLS (mean ± SD, $n = 3$); C) colloidal long-term stability of Zr-PMX@TMSP NPs (-$pGlu_{31}$-*b*-$pSar_{160}$-N_3) and polymer-coated Zr-PMX@TMSP NPs (+$pGlu_{31}$-*b*-$pSar_{160}$-N_3) in HBG (mean ± SD, $n = 3$) or (D) PBS (mean ± SD, $n = 3$) at 37 °C; E) serum stability of the polymer coating visualized by CLSM. Green channel, NP core labeled by coordinative integration of calcein. Red channel, polymer shell labeled with Alexa Fluor 647. Yellow signal in the merged channel indicates co-localization of NP core and polymer shell. "All channels": includes nuclei stained with DAPI (blue) and actin stained with phalloidin-rhodamine (white).

overexpressed by cancer cells and undergoes rapid and efficient internalization upon ligand binding.[51] Coating Zr-PMX@TMSP NPs with low amounts of 5 µg or 10 µg pGlu-*b*-pSar-Tf (Figure 6A) led to gradual increases in *z*-average and PDI, but suitable NPs featuring a small *z*-average, narrow size distribution and neutral zeta potential could be obtained by coating with 25 µg pGlu-*b*-pSar-Tf (Figure 6B). After confirming transferrin receptor expression levels (Figure S11, Supporting Information), confocal microscopy uptakes experiments with 1 h of incubation revealed a transferrin targeting effect on both KB (Figure 6C) and A549 cells (Figure 6D). For both cell lines, the green calcein signal representing labeled NP cores was more pronounced for Tf-targeted NPs when compared to the untargeted NPs coated with pGlu-*b*-pSar. Repeating the confocal microscopy experiment with a reduced incubation time of 15 min in order to elucidate the uptake kinetics (Figure S12, Supporting Information) led to a similar result although the effect of the transferrin targeting became less prominent due to the shorter NP exposure. Quantitative evaluation by flow cytometry (Figure 6E) also showed a slight shift of the cell population toward higher calcein fluorescence at the early time point.

We also determined the cell killing potential of the NP formulations using PMX sensitive L1210 and rather insensitive KB cells. Initially, PMX dose–response (Figure S13 and S14, Supporting Information) and incubation time studies (Figure S15 and S16, Supporting Information) were performed on both cell lines to define the assay parameters and effective concentration ranges of PMX. Treatment of KB cells revealed preserved activity of Zr-PMX NPs compared to free PMX and a slight increase in toxicity of folate- and transferrin-targeted formulations after a short exposure time of 1 h (Figure 5E and 6F). A faster uptake kinetic of the targeted nanoformulations compared to free PMX could be a possible reason for the observation; the absence of different toxicities on KB cells after 72 h of incubation indicates that potential benefits of the targeted nanoformulations can indeed rather be expected at early time points. Preserved activity of PMX in the nanoformulations was also confirmed for the highly sensitive L1210 cells with 1 h of NP or drug exposure time (Figure 5E). After 72 h, (Figure S16, Supporting Information) Zr-PMX NPs even mediated an increased toxicity at the low concentration of 1 nM (>60% reduced viability). However, since PMX is a potent cytotoxic drug with high activity on L1210 cells, uptake kinetics do not seem to represent a major limiting factor for this cell line and the advantage of targeted nanoformulations can hardly be assessed under the static cell culture conditions.

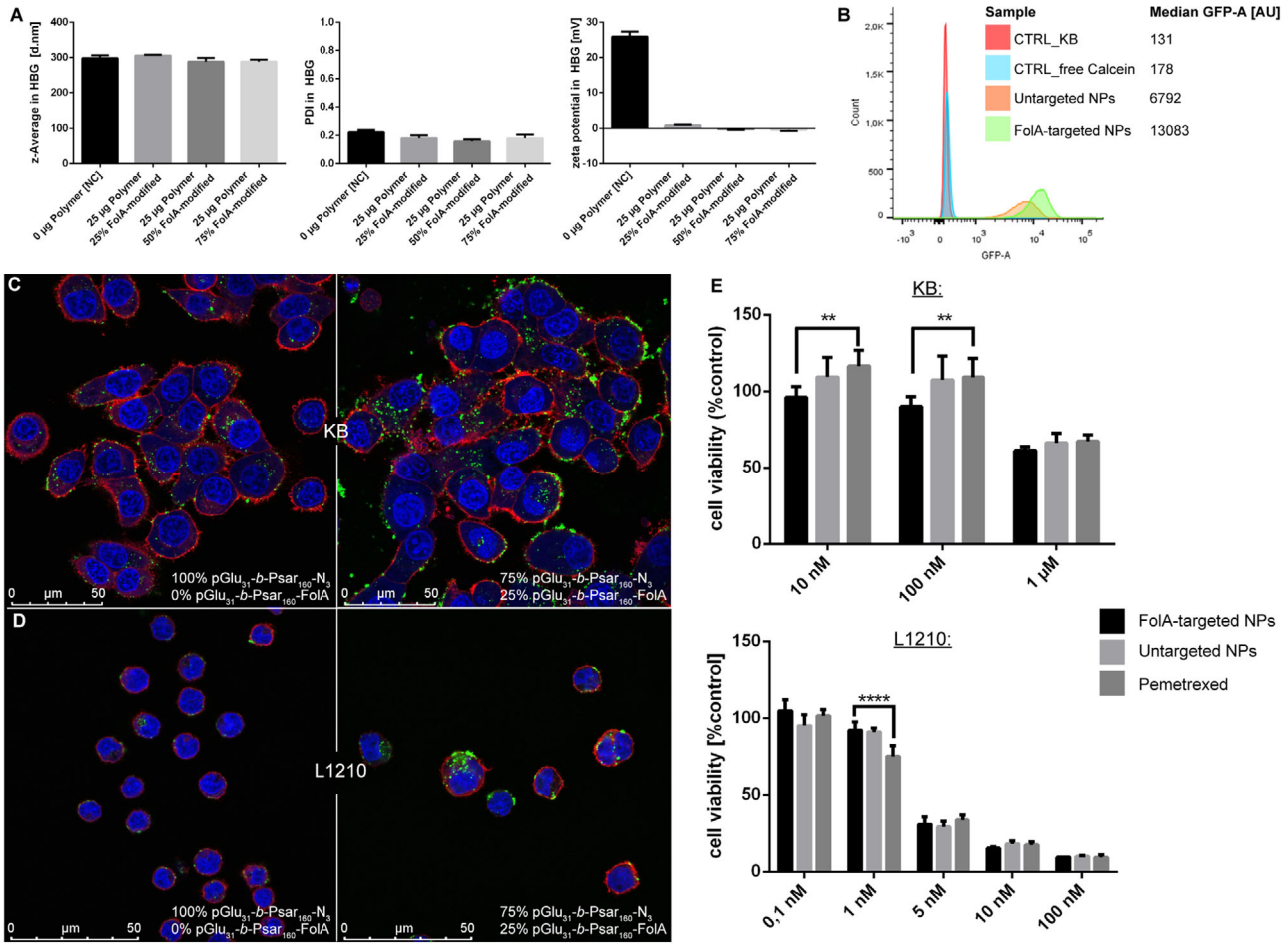

Figure 5. Folate-targeting mediated by coating with pGlu-*b*-pSar-FolA. A) Polymer dose titration and influence on size, polydispersity, and zeta potential by DLS (mean ± SD, $n = 3$); B) effects of FolA-targeting on NP uptake by flow cytometry; C) evaluation of NP uptake into KB; or (D) L1210 cells for FolA-targeted and untargeted NPs by CLSM. Green, NP core labeled by coordinative integration of calcein. Red, actin stained with phalloidin-rhodamine. Blue, nuclei stained with DAPI. E) Cell viability studies with KB (top) and L1210 (bottom) by MTT-assay (mean ± SD, $n = 5$). Cells were treated with NPs or free drug for 1 h, then the medium was changed and the readout took place after 72 h. PMX content of NPs was quantified by HPLC and the dosing adjusted accordingly. Statistical analysis was performed by two-way ANOVA, $\alpha = 0.05$.

3. Conclusions

In sum, a novel approach for the assembly and subsequent core-shell functionalization of a drug carrier with a very high loading capacity, tunable stabilization against serum, surface shielding and the option for receptor targeting is presented. The drug-containing core consists of PMX and Zr ions which assemble into nanocolloids via Lewis acid–base interactions. The absence of crystallinity suggests that the mesoporous Zr-PMX NPs can rather be classified as amorphous coordination polymers. Since PMX displays a high binding affinity toward serum protein, the particles disassemble rapidly in a serum-containing environment and require a thin TMSP-based silica shell for stabilization and simultaneous control of drug release. A pGlu-*b*-pSar-N_3 block-copolymer represents the outermost layer of the delivery system, mediates surface shielding, highly efficient colloidal stabilization and enables modification with uptake-enhancing receptor ligands as shown for folate and transferrin. In vitro evaluations confirmed the maintained pharmacological activity of PMX on KB human cervix carcinoma and L1210 mouse lymphocytic leukemia cells and the cellular uptake of otherwise impermeable coencapsulated calcein. The presented concept is considered to be an example of an envisioned "minimalist design" of nanopharmaceuticals with a very high drug-to-carrier material ratio meant to minimize patient exposure to inactive carrier materials.

4. Experimental Section

Materials and Reagents: Pemetrexed disodium heptahydrate (PHR1596), zirconium(IV)chloride, transferrin from human plasma, DBCO-PEG_4-NHS, N^1-(3-trimethoxysilylpropyl)diethylenetriamine, DBCO-PEG_4-NHS, and calcein were obtained from Sigma–Aldrich (Germany). Ethanol absolute and HCl 37% were obtained from VWR chemicals. DBCO-FolA used to generate pGlu-pSar-FolA was synthesized in house as reported earlier.[49] HEPES was purchased from Biomol, formic acid (≥ 99.5%) was bought from Fluka (Buchs, Switzerland), DBCO-Alexafluor647 was purchased from Jena Biosciences (Jena,

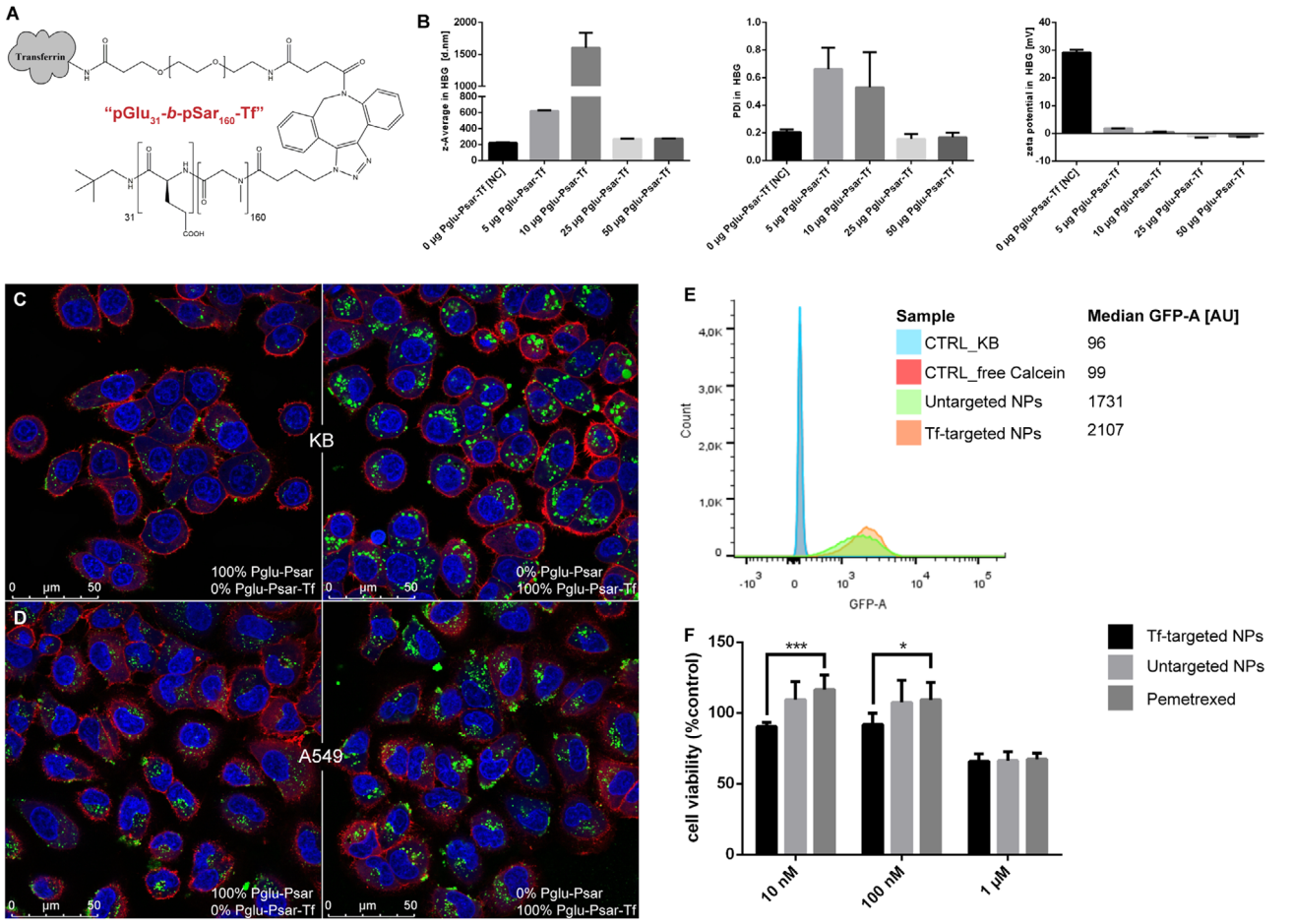

Figure 6. Transferrin targeting mediated by coating with pGlu-*b*-pSar-Tf. A) Structure of pGlu-*b*-pSar-Tf; B) polymer dose titration and influence on size, polydispersity, and zeta potential by DLS (mean ± SD, $n = 3$); C) evaluation of NP uptake into KB; or (D) A549 cells for Tf-targeted and untargeted NPs by CLSM. Green, NP core labeled by coordinative integration of calcein. Red, actin stained with phalloidin-rhodamine. Blue, nuclei stained with DAPI. E) Effects of Tf-targeting on NP uptake by flow cytometry and F) cell viability studies with KB by MTT-assay (mean ± SD, $n = 5$). Cells were treated with NP or free drug for 1 h, then the medium was changed and the readout took place after 72 h. PMX content of NPs was quantified by HPLC and the dosing adjusted accordingly. Statistical analysis was performed by two-way ANOVA, $\alpha = 0.05$.

Germany),FBS and cell culture mediums were bought from Life Technologies (USA) or Sigma-Aldrich. HBG buffer pH 7.4 containing 20 mM HEPES, 5% glucose (w/v), and 20 mM PBS pH 7.4 were prepared in-house. All used water was generated utilizing the Milli-Q Academic A-10 system from Millipore (Billerica, USA).

Synthesis of Zr-PMX NPs: A mixture of 416 µL 10 mM $ZrCl_4$ (1 eq., 4.16 µmol, freshly dissolved in bidistilled water), 50 µL 1 M HCl and 48.5 µL formic acid (100 eq.) was prepared in a 50 mL falcon tube and stirred at medium speed using a magnetic stirrer (solution I). In a separate 5 mL tube, 488 µL 15 mg mL^{-1} pemetrexed disodium heptahydrate (3 eq., 12.48 µmol, dissolved in bidistilled water) was mixed with 3 mL EtOH absolute (solution II). Solution II was then quickly added to solution I while stirring. The mixture was further stirred at medium speed for 45 min. Afterward, the reaction batch was split into three 1.5 mL polystyrene microcentrifuge tubes and centrifuged (Eppendorf tabletop centrifuge,14 000 rpm, 1 min, Eppendorf GmbH, Hamburg, Germany). The supernatants were removed and the three pellets were unified in 1 mL fresh EtOH absolute. The concentrated NP stock solution was then washed an additional two times with EtOH absolute (1 mL EtOH absolute and 1 min @ 14 000 rpm centrifugation per washing step). The washed NPs were redispersed in 1 mL EtOH absolute by gentle pipetting and subsequently sonicated for 5 min (20 °C, power 9) using a VWR USC THD/HF Ultrasonic Cleaner (VWR International GmbH, Darmstadt, Germany).

Synthesis of Zr-Calcein-PMX NPs: Zr-PMX NPs containing calcein were prepared identically to Zr-PMX NPs with the exception of solution II additionally containing 17.85 µM calcein (12.5 µL 5 mM calcein were added to solution II prior to mixing solutions I and II).

Dynamic Light Scattering: Size and zeta-potential measurements were performed at a backscattering angle of 173° using the Nano Series Nano-ZS Zetasizer equipped with DTS-1070 folded capillary cuvettes (Malvern Instruments, Malvern, Worcestershire, United Kingdom). For size measurements, an equilibration time of 0 s was set and the attenuator was adjusted automatically. Measurements in HEPES-buffered glucose were performed at 25 °C with a solvent refractive index of 1.330 whereas a temperature of 20 °C and a solvent refractive index of 1.3617 were used for EtOH. Each sample was measured three times with at least six subruns each and *z*-averages, PDIs, and zeta potentials were reported as mean ± standard deviation. Zeta potential measurements were carried out in HEPES-buffered glucose as triplicates with 10–15 subruns each and the actual zeta potential values were calculated by the zetasizer software by applying the Smoluchowski equation.

Determination of Zirconium Content by ICP-AES: A total of 1 mL Zr-PMX NPs in EtOH was transferred to a weighed polystyrene microcentrifuge tube, centrifuged (1 min, 14 000 rpm, Eppendorf tabletop centrifuge) and the supernatant was carefully discarded. The NP pellet was then dried under high vacuum for approximately 24 h followed by

approximately 4 h drying at 90 °C. Next, the Eppendorf caps were weighed again and the dried NPs were digested in 69% (v/v) HNO_3 for trace analysis (Aristar, VWR) and subsequently diluted with bidistilled water to 3% (v/v) HNO_3. The samples were then analyzed for their Zirconium content by ICP-AES (CCD simultaneous ICP AES Vista RL by Agilent, suction time 35 s, stabilization time 45 s, power 1.25 kW). The following wavelengths were determined: 257.47, 327.307, 339.198, 343.823, and 349.619. Utilizing this method, three independent samples were prepared and analyzed and the zirconium content was reported as average mass percentage ± standard deviation.

Determination of PMX Content by HPLC: Zr-PMX NPs in EtOH were synthesized as described above. A total of 200 µL of the synthesized Zr-PMX NPs in EtOH was then mixed with 1 mL 500 mM EDTA pH 8.2 and 300 µL bidistilled water. Three independent samples were prepared and incubated for 72 h at 25 °C under constant shaking (500 rpm, Eppendorf tabletop shaker, Eppendorf GmbH, Hamburg, Germany). In order to avoid EDTA precipitation under acidic conditions, the lysed NPs were subsequently diluted with an equal volume of 0.1% (v/v) trifluoroacetic acid (TFA) in bidistilled water and the PMX released from the NPs was then quantified by HPLC (Hitachi Chromaster, YMC RP-18 column, 50 µL injection volume, PMX retention time 10.847 min, monitoring @ 225 nm, solvents bidistilled water + 0.1% TFA, HPLC-grade acetonitrile (ACN) + 0.1% TFA (0–2.5 min: 1% ACN + 0.1% TFA, 2.5–11 min: increase to 41.4%, 11–12 min: increase to 100%, 12–14 min: wash with 100%). Using a PMX calibration curve and the PMX molecular weight of 427.411 g mol^{-1}, the mass of PMX present in each sample was calculated. To obtain the drug loading of PMX within the NP, the total mass of NP present in each sample was determined by transferring 1 mL Zr-PMX NPs in EtOH to a weighed 1.5 mL polystyrene microcentrifuge tube, centrifuging (1 min, 14 000 rpm, Eppendorf tabletop centrifuge) and removing the supernatant very carefully to avoid loss of material. The NP pellet was then dried under high vacuum for approximately 48 h followed by approximately 4 h drying at 90 °C. The average of three mass determinations was then used to calculate the mass of NP present in each HPLC sample. The fraction of PMX in the NP (w/w) was subsequently calculated according to the following formula: [µg PMX in the HPLC sample/µg NP in the HPLC sample] × 100%.

Scanning Electron Microscopy (SEM): The respective NP stock solutions in EtOH were concentrated approximately tenfold (by centrifugation and redispersion in a smaller volume of EtOH) and subsequently spotted onto a hydrophobic SEM sample carrier. After drying overnight in a dust protected environment, the samples were sputtered with carbon (three cycles of carbon vacuum deposition) and their morphology was then characterized using a Dual beam FEI Helios G3 UC SEM operated at 3 kV. Particle sizes were determined by recording high-resolution images, correcting them for contrast and brightness and subsequently measuring 100 particles using the ImageJ software (version 1.50i). The obtained sizes were reported in nanometers as average ± standard deviation. The elemental composition was analyzed during SEM measurements by energy dispersive X-ray spectroscopy (EDX) using an Oxford Instruments X-Max N80 device.

X-ray Diffraction: XRD was measured with a Stadi MP STOE transmission diffractometer system with Cu Kα1 radiation (λ = 1.54060 Å) and a Ge(111) single crystal monochromator. All samples were prepared by fixating the dried samples between two polymer foils. Diffraction patterns were recorded with a DECTRIS solid-state strip detector MYTHEN 1K in a transmission setup derived from Debye–Scherrer geometry using a step size of 4.71° and a counting time of 120 s per step. For data analysis, the WinXPOW RawDat v3.0.2.5 software package was used.

BET Sorption Measurements: The nitrogen sorption isotherm was measured at 77 K with a Quantachrome Autosorb-1 iQ. Approximately 7.3 mg dried NPs was degassed at 60 °C under high vacuum for 38 h prior to the measurement. Evaluation of the sorption data was carried out using the ASiQwinTM software (Version 3.0, Quantachrome Instruments). BET surface areas were calculated employing the linearized form of the BET equation. With a relative pressure range between 0.15 and 0.27, this resulted in a correlation coefficient >0.999 with a positive *C* constant. The adsorption isotherm was then used to calculate the pore size distribution by employing the quenched solid density functional theory (QSDFT, N_2 at 77 K on carbon, cylindrical pores adsorption branch).

Thermogravimetric Analysis: Thermogravimetric analysis was carried out with a thermomicrobalance (Netzsch, STA 449 C Jupiter) by applying a heating rate of 10 °C min^{-1} up to 900 °C. A total of 7.425 mg of material was heated under synthetic air (N_2/O_2 mixture) with a flow rate of 25 mL min^{-1}. For data evaluation, the Proteus—Thermal Analysis (v.4.3) software was used.

TMSP-coating of Zr-PMX NPs: A mixture of 1 mL EtOH absolute and 3 µL TMSP was prepared in a 50 mL falcon tube and stirred at low to medium speed with a magnetic stirrer. In a separate vial, 400 µL Zr-PMX-NPs in EtOH were prediluted with 2 mL ethanol absolute and briefly vortexed. The prediluted Zr-PMX NPs were then added dropwise to the diluted TMSP solution within approximately 2 min and stirred for 5 min at low to medium speed. After 5 min, the polymerization process was initiated by addition of 60 µL 5M HCl. The tube was then stirred at low to medium speed for 3 h. Afterward, the reaction batch was split into three 1.5 mL polystyrene microcentrifuge tubes, centrifuged (1 min, 14 000 rpm, Eppendorf tabletop centrifuge) and the three pellets were unified in 1 mL fresh EtOH absolute. The sample was washed two more times with EtOH absolute (1 mL, 1 min@14 000 rpm, Eppendorf tabletop centrifuge). After the final washing step, the pellet was redispersed in 1 mL EtOH absolute and sonicated for 5 min (20 °C, power9) using the VWR USC THD/HF Ultrasonic Cleaner (VWR International GmbH, Darmstadt, Germany). Zr-Calcein-PMX NPs were coated with TMSP using the same protocol.

Serum Stability of Zr-PMX@TMSP NPs: For each sample, 1 mL of Zr-Calcein-PMX@TMSP NPs in EtOH was centrifuged (1 min, 14 000 rpm, Eppendorf tabletop centrifuge) and the supernatant was removed carefully to avoid loss of material. The pellet was then redispersed in 1 mL 10% (v/v) fetal bovine serum and subsequently incubated at 37 °C for 30 min. After the incubation, the samples were centrifuged (5 min, 14 000 rpm, Eppendorf tabletop centrifuge) and 100 µL of supernatant was diluted with 100 µL 0.1% (v/v) TFA in bidistilled water. The amount of released PMX present in the supernatant was then quantified by HPLC using a sample volume of 100 µL and the instrumentation described in section "Determination of PMX Content by HPLC." To obtain 100% release values to normalize to, a triplicate with respective equal amounts of NP was centrifuged (1 min, 14 000 rpm, Eppendorf tabletop centrifuge), the supernatants were carefully discarded and the pellets were redispersed in 1 mL lysis buffer (500 mM EDTA pH 8.2) and incubated approximately 72 h (37 °C, 500 rpm). The set was then quantified by HPLC and the average of the determined PMX content was used as 100% value. The amount of released PMX for the serum-incubated samples was then calculated according to the following formula: [PMX in supernatant/PMX in lysis sample] * 100%. For each time point, a set of independent triplicates was prepared and analyzed and the percentage of released PMX was reported as average ± standard deviation.

Synthesis of $pGlu_{31}$-b-$pSar_{160}$-N_3: All monomers were prepared according to the Fuchs–Farthing method with diphosgene as phosgene source and purified by recrystallization (Glu(O^tBu)-NCA) or sublimation (SarNCA) as reported previously.[40,52] The synthetic pathway to azide-modified poly(L-glutamic acid)-*block*-poly(sarcosine) was adapted and modified from Yoo et al. and Schäfer et al.[53]

Briefly, poly(γ-*tert*-butyl-L-glutamic acid)-*block*-poly(sarcosine) (pGlu(O^tBu)-*b*-pSar) was prepared via sequential *N*-carboxyanhydride (NCA) polymerization initiated by neopentylamine. A total of 407.6 mg (1.78 mmol; 31 eq.) of γ-*tert*-butyl-L-glutamic acid (Glu(O^tBu))-NCA was weighed into a pre-dried Schlenk-flask, dissolved in mixture of 1:1 THF and DMF (both dried and freshly distilled) at a concentration of 100 g L^{-1}, cooled to 0 °C, and a solution of neopentylamine (5.0 mg; 57.4 µmol; 1.0 eq.) in 0.5 mL of DMF was added. After completed Glu(O^tBu)-NCA consumption, as monitored by FT-IR spectroscopy, a solution of sarcosine-NCA (1.06 g; 9.17 mmol; 160 eq.) in 5.0 mL of DMF was added and the polymerization was continued at 10 °C. For azide end-group modification, pentafluorphenyl-4-azidobutanoate (33.9 mg; 0.115 mmol, 2.0 eq.) and *N,N*-diisopropylethylamine (DIPEA) (53 µL; 0.304 mmol; 5.0 eq.) were added and the solution was stirred at room temperature for 18 h. To react residual-free end groups, acetic anhydride (54 µL; 0.57 mmol; 10 eq.)

and DIPEA (195 µL; 1.11 mmol; 20 eq.) were added and the solution was stirred for 1 day. The obtained block copolymer was purified by repetitive (3×) precipitation/centrifugation (4500 rpm, 15 min, 4 °C) into a mixture of *n*-hexane and diethyl ether (2:1). The product (pGlu $(O^tBu)_{31}$-*b*-$pSar_{160}$-N_3) was dried in vacuo and obtained as a white powder (846 mg, 86%).

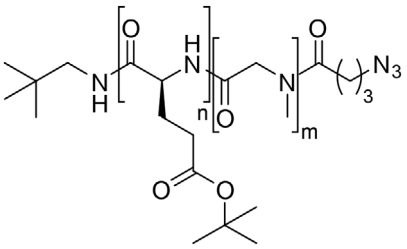

^{1}H NMR: pGlu $(O^tBu)_n$-*b*-$pSar_m$-N_3 (400 MHz, CD_2Cl_2), δ [ppm] = 8.45–8.11 (22 H, br, –**NH**–CO–CH–), 4.40–3.82 (323 H (1n + 2m), br, –CO–**CH**–NH + –CO–**CH_2**–NCH_3–), 3.20–2.80 (454 H (3m), m, –**NCH_3**–CO–), 2.66–1.70 (140 H, m, –**CH_2**–**CH_2**–), 1.53–1.36 (285 H, s + br, –**O–C$(CH_3)_3$**), 0.94–0.83 (9 H, br CH_2–**C$(CH_3)_3$**). HFIP-GPC: Mn = 39.5 kg mol^{-1}, Mw = 45.4 kg mol^{-1}; Đ = 1.15.

For deprotection, 800 mg of pGlu $(O^tBu)_{31}$-*b*-$pSar_{160}$-N_3 was dissolved in 16 mL of a mixture of 45:45:5:5 DCM/TFA/TIPS/water over 3 h in a Schlenk-flask with constant stirring. Polymers were precipitated into ether, centrifuged in sealed Falcon tubes and the precipitate was dialyzed against aqueous $NaHCO_3$ and water, followed by lyophilization (yield 80%). Successful deprotection was verified by ^{1}H NMR.

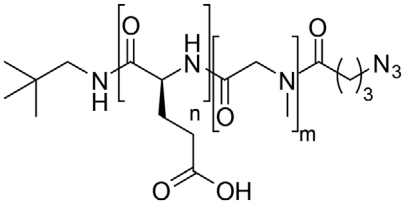

^{1}H NMR: pGlu $(COOH)_n$-*b*-$pSar_m$-N_3 (400 MHz, D_2O), δ [ppm] = 4.50–4.00 (490 H, (1n + 2m), m, HN–**CH_2**–CO + HN–**CH**–CO), 3.30–2.72 (669 H (3m), m **NCH_3**), 2.33–1.70 (195 H (2n), m, **CH_2**–**CH_2**), 0.77-0.71 (9H, s, –**C$(CH_3)_3$**). HFIP-GPC: Mn = 29.4 kg mol^{-1}, Mw = 35.1 kg mol^{-1}; Đ = 1.19.

HFIP-GPC:

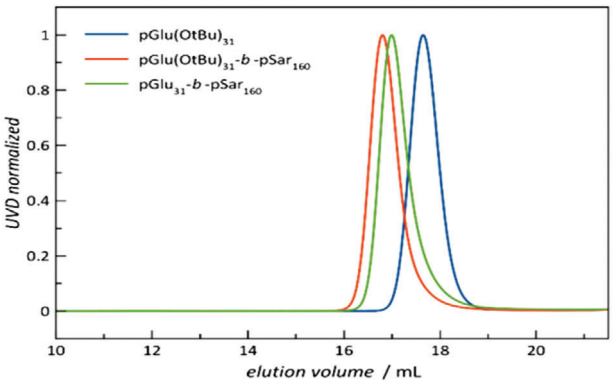

Synthesis and Purification of $pGlu_{31}$-b-$pSar_{160}$-Folate: $Pglu_{31}$-$Psar_{160}$-FolA was synthesized by reacting $pGlu_{31}$-*b*-$pSar_{160}$-N_3 with a DBCO-Folate conjugate, referred to here as DBCO-FolA, (folic acid-lysine-DBCO; gamma-COOH of folic acid coupled to alpha-amine of lysine, epsilon-amine of lysine coupled to DBCO-carboxylic acid).[49] A total of 3 mg $pGlu_{31}$-*b*-$pSar_{160}$-N_3 (1 eq., 189.9 nmol) was dissolved in 168 µL 1 mg mL^{-1} DBCO-FolA (1 eq, 189.9 nmol) in HBG (20 mM, pH 7.4). The mixture was incubated overnight and dialysed for 2 days at 4 °C against Millipore-water. A Spectra/Por prewetted RC tubing dialysis membrane with a molecular weight cutoff of 2 kD was used and the water was changed once after approximately 24 h. The purified compound was snap frozen in liquid nitrogen, freeze-dried (Christ Alpha 2–4 LD plus, Martin Christ, Gefriertrocknungsanlagen GmbH, Osterode, Germany) and dissolved in bidistilled water at 1 mg mL^{-1}.

Synthesis and Purification of $pGlu_{31}$-b-$pSar_{160}$-Transferrin: Transferrin from human plasma (50 mg, 1 eq., 0.67 µmol) was dissolved in 1 mL HEPES buffer (20 mM, pH 7.4). DBCO-PEG_4-NHS ester was dissolved in DMSO (20 mg mL^{-1}) and 43.5 µL (0.87 mg, 2 eq., 1.3 µmol) was added to the transferrin solution. The reaction mixture was incubated for 3 h at room temperature under gentle shaking (25 °C, 400 rpm). The solution was then purified by size exclusion chromatography using an ÄKTA purifier system (GE Healthcare), a Sephadex G25 super fine-size exclusion column and HEPES buffer (20 mM, pH 7.4) as a mobile phase. The collected fractions containing the DBCO-modified transferrin were pooled and the protein concentration was determined by Bradford assay.[54] By pooling the fractions, 4.75 mL DBCO-PEG_4-transferrin with a concentration of 105 µM corresponding to a total yield of approximately 79% was obtained. Next, $pGlu_{31}$-*b*-$pSar_{160}$-N_3 (3 mg, 1.1 eq., 189.9 nmol) was dissolved in 1.81 mL of the obtained DBCO-PEG_4-transferrin (1 eq., 209 nmol) and the mixture was incubated overnight. The resulting transferrin-modified polymer was diluted with HEPES to a final concentration of 1 mg mL^{-1}, used without further purification and stored at 4 °C.

Synthesis and Purification of $pGlu_{31}$-b-$pSar_{160}$-AF647: DBCO-AlexaFluor647 (Jena Bioscience GmbH, Jena, Germany) was dissolved in DMSO at 1 mg mL^{-1}. A total of 455 µL of the dissolved DBCO-Alexafluor647 (1.2 eq., 403 nmol) was then used to dissolve 5.3 mg $pGlu_{31}$-*b*-$pSar_{160}$-N_3 (1 eq., 335 nmol). The obtained mixture was then incubated overnight in an Eppendorf tabletop shaker (25 °C, 400 rpm). On the next morning, the product was dialyzed for about 48 h at 4 °C against bidistilled water. Prior to adding the reaction batch to the dialysis membrane (Spectra/Por prewetted RC Tubing, MWCO 2 kD), the membrane was rinsed with bidistilled water to remove the azide antifouling agent and bidistilled water was then added to the sample to reduce the DMSO content to approximately 20% v/v as a precaution in order to safeguard membrane integrity. During the dialysis step, the water was changed once after approximately 12 h, minor precipitation of blue product within the dialysis bag was observed. After dialysis, the sample was snap frozen in liquid nitrogen and freeze-dried over 2 days (Christ Alpha 2–4 LD plus, Martin Christ, Gefriertrocknungsanlagen GmbH, Osterode, Germany) and dissolved in bidistilled water at a final concentration of 1 mg mL^{-1}.

Uptake Experiments by CLSM: The respective cells were seeded in eight well-chamber slides (Thermo Fisher Scientific, 20.000 cells in 300 µL medium per well) 1 day prior to recording the images and cultured at 37 °C and 5% CO_2. On the day of the experiment, the medium was exchanged for 240 µL of fresh medium. The NPs were added in 60 µL HBG per well. After 1 h of incubation, the treatment solutions were replaced with fresh medium and the cells were incubated for additional 2 h at 37 °C and 5% CO_2. Cells were then fixated with 4% paraformaldehyde in PBS (30 min incubation, room temperature). After fixating the cells, each well was washed once more with 400 µL PBS. Nuclei were stained with DAPI (2 µg mL^{-1}) and F-Actin was labeled with phalloidin-rhodamine (1 µg mL^{-1}). After 30 min of light-protected incubation at room temperature, the staining mixture was removed and replaced with 300 µL PBS per well. Images were then recorded on a Leica-TCS-SP8 confocal laser scanning microscope equipped with an HC PL APO 63 × 1.4 objective. DAPI emission was recorded at 460 nm and calcein at 530 nm. All images were processed utilizing the LAS X software from Leica.

$pGlu_{31}$-b-$pSar_{160}$-N_3 Coating of Zr-PMX@TMSP NPs: $pGlu_{31}$-*b*-$pSar_{160}$-N_3 was prepared as an aqueous 1 mg mL^{-1} stock solution. For the dose titration studies, x µL polymer corresponding to *x* µg polymer was added to a 5 mL polystyrene tube and stirred at medium speed. Next, ethanolic Zr-PMX@TMSP NPs were centrifuged (1 min, 14 000 rpm, Eppendorf tabletop centrifuge). The supernatant was carefully removed and the particles were redispersed in an equal volume of HBG (20 mM,

pH 7.4). The particles in HBG were then sonicated for 1 min. Next, 500 µL of Zr-PMX@TMSP NPs in HBG were added dropwise to the stirred polymer solution over approximately 2 min. The solution was stirred for additional 3 min and the obtained polymer-coated Zr-PMX@TMSP NPs were sonicated for 1 min (power 9, 20 °C) using the VWR USC THD/HF Ultrasonic Cleaner (VWR International GmbH, Darmstadt, Germany).

$pGlu_{31}$-b-$pSar_{160}$-FolA Coating of Zr-PMX@TMSP NPs: To obtain folate-targeted Zr-PMX@TMSP NPs, a mixture of 1 mg mL^{-1} $Pglu_{31}$-$Psar_{160}$-N_3 and 1 mg mL^{-1} $pGlu_{31}$-*b*-$pSar_{160}$-FolA was prepared in a 5 mL Eppendorf tube stirred at medium speed. A total of 500 µL of Zr-PMX@TMSP NPs in HBG was added dropwise to the stirred polymer solution over approximately 2 min. The solution was stirred for an additional 3 min and the obtained polymer-coated Zr-PMX@TMSP NPs were sonicated for 1 min (power 9, 20 °C) using the VWR USC THD/HF Ultrasonic Cleaner (VWR International GmbH, Darmstadt, Germany). For the dose titration experiment, a total of 25 µL polymer containing various percentages $pGlu_{31}$-*b*-$pSar_{160}$-FolA was used. For the uptake experiments by confocal microscopy and the MTT assay, 500 µL of Zr-PMX@TMSP NPs in HBG was coated with a fixed amount of 25 µg polymer containing 25% folate-modified polymer (6.25 µL 1 mg mL^{-1} $pGlu_{31}$-*b*-$pSar_{160}$-FolA + 18.75 µL $pGlu_{31}$-*b*-$pSar_{160}$-N_3) as described above.

$pGlu_{31}$-b-$pSar_{160}$-Transferrin Coating of Zr-PMX@TMSP NPs: To obtain transferrin-targeted Zr-PMX@TMSP NPs *x* µL 1 mg mL^{-1} $pGlu_{31}$-*b*-$pSar_{160}$-transferrin (nomalized to polymer content) was prepared in a 5 mL polystyrene microcentrifuge tube stirred at medium speed. A total of 500 µL of Zr-PMX@TMSP NPs in HBG was added dropwise to the stirred polymer solution over approximately 2 min. The solution was stirred for another 3 min and the obtained polymer-coated Zr-PMX@TMSP NPs were sonicated for 1 min (power 9, 20 °C) using the VWR USC THD/HF Ultrasonic Cleaner (VWR International GmbH, Darmstadt, Germany). For the dose titration experiment, various amounts (0– 50 µL) $pGlu_{31}$-*b*-$pSar_{160}$-transferrin were used. For the uptake experiments by confocal microscopy, 500 µL of Zr-PMX@TMSP NPs in HBG was coated with a fixed amount of 25 µg $pGlu_{31}$-*b*-$pSar_{160}$-transferrin as described above.

Colloidal Stability Studies of Zr-PMX@TMSP-NPs ± $pGlu_{31}$-b-$pSar_{160}$-N_3: For the HBG stability experiment, 500 µL Zr-PMX@TMSP NPs in HBG were coated with 25 µg $pGlu_{31}$-*b*-$pSar_{160}$-N_3 as described above and incubated using an Eppendorf tabletop shaker (37 °C, 400 rpm). Every 24 h, 75 µL sample was drawn, diluted with 645 µL HBG and size, PDI and zeta-potential were determined by DLS. For the PBS stability experiment, Zr-PMX@TMSP-NPs were coated with 25 µg $pGglu_{31}$-*b*-$pSar_{160}$-N_3 and incubated as described above. Then, 200 µL of the coated NPs in HBG were added to 800 µL PBS (20 mM, pH 7.4). Every 24 h, 180 µL sample was withdrawn, diluted with 540 µL PBS and then the size, PDI, and zeta potential were determined as described earlier.

Serum Stability of the Polymer Coating: In a 5 mL polystyrene microcentrifuge tube, 25 µL $pGlu_{31}$-*b*-$pSar_{160}$-AF647 was stirred at medium speed. A total of 500 µL Zr-PMX@TMSP NPs in HBG was added dropwise to the stirred polymer solution over approximately 2 min. The solution was stirred for another 3 min and the obtained polymer-coated Zr-PMX@TMSP NPs were sonicated for 1 min (power 9, 20 °C) using the VWR USC THD/HF Ultrasonic Cleaner (VWR International GmbH, Darmstadt, Germany). One day prior to recording the images, KB cells were seeded in eight well-chamber slides (Thermo Fisher Scientific, 20 000 cells in 300 µL medium per well) and cultured at 37 °C and 5% CO_2. On the day of the experiment, the medium was removed, replaced with 240 µL fresh medium and 60 µL NPs dispersed in HBG were added. After 2 h of incubation at 37 °C and 5% CO_2, each well was emptied by aspiration, supplemented with fresh medium, and incubated for another 2 h. The cells were then fixated with 4% paraformaldehyde in PBS (30 min incubation, room temperature). After fixating the cells, each well was washed once more with 400 µL PBS. Cell nuclei were then stained with DAPI (2 µg mL^{-1}) and F-Actin was labeled with phalloidin-rhodamine (1 µg mL^{-1}). After 30 min of incubation (room temperature, light protection), the staining mixture was removed and replaced with 300 µL PBS per well. Images were generated on a Leica-TCS-SP8 confocal laser scanning microscope equipped with an HC PL APO 63 × 1.4 objective. DAPI emission was recorded at 460 nm, calcein at 530 nm, rhodamine at 580 nm, and Alexafluor647 at 667 nm. All images were processed with the LAS X software from Leica.

Evaluation of Toxicity by MTT-assay (KB Adherent Cells): A total of 5 000 KB cells/well were seeded in 96-well plates (Corning® Costar, Sigma–Aldrich, Germany) 1 day prior to the experiment. The respective amount of formulation to be tested was prepared in HBG pH 7.4 at a fivefold concentration. For each well, 100 µL of treatment solution was prepared by mixing 20 µL formulation in HBG with 80 µL medium. After 24 h seeding the cells, the medium was aspirated and replaced with 100 µL treatment solution. For each formulation and concentration, an independent quintuplicate of five wells was treated. After addition of the treatment, the cells were incubated for the indicated duration at 37 °C and 5% CO_2. Afterward, the wells were aspirated and replaced with fresh medium. After 72 h addition of the sample solutions, 10 µL MTT (3-(4,5-dimethylthiazol-2-yl)-2,5-diphenyltetrazolium bromide) (5 mg mL^{-1}) resulting in a final concentration of 0.5 mg mL^{-1} was added to each well. The plates were then incubated for 2 h at 37 °C under mild shaking. Unreacted dye and medium were subsequently aspirated and the 96-well plates frozen at −80 °C for approximately 2 h. In order to fully dissolve the purple formazan product, 100 µL DMSO was added to each well. The plates were then incubated under agitation for another 30 min. By measuring the absorbance at 590 nm taken together with a background correction at 630 nm using a microplate reader (TecanSpectrafluor Plus, Tecan, Switzerland), the absorption of each well was quantified. The relative cell viability (%) related to control wells treated with 20 µL HBG (pH 7.4) was then calculated as ([*A*] test/[*A*] control) × 100%.

Evaluation of Toxicity by MTT-assay (L1210 Suspension Cells): L1210 cells were withdrawn from their culture flask, centrifuged (1500 rpm, 5 min), washed, resuspended in folate-free medium and cultured for 24 h at 37 °C and 5% CO_2. Afterward, the cell density was determined and adjusted to 125 000 cells mL^{-1}. Treatment solutions in HBG buffer were prepared at fivefold their intended final concentration. A total of 480 µL cell suspension (125 000 cells mL^{-1}) was then mixed with 120 µL respective treatment solution prepared at fivefold concentration. The obtained 600 µL cell suspension now containing the treatment at the final onefold concentration was then transferred to five adjacent wells of a 96-well plate(100 µL corresponding to 10 000 L1210 cells were added to each well). The cells were then cultured for the indicated duration at 37 °C and 5% CO_2. For the 1 + 71 h incubation, cells were washed after 1 h by centrifuging (1500 rpm, 5 min) and replacing 50 µL of supernatant with fresh folate-free medium. This step was performed twice. After 72 h addition of the sample solutions, 100 µL of lysis buffer (10 mM HCl, 10% w/v sodiumdodecylsulfate) was added to each well. The plates were then incubated for 2 h (37 °C, 5% CO_2). Absorption values were then determined at 590 nm taken together with a background correction at 630 nm using a microplate reader (TecanSpectrafluor Plus, Tecan, Switzerland). The relative cell viability (%) related to control wells treated with 20 µL HBG (pH 7.4) was then calculated as ([*A*] test/[*A*] control) × 100%.

NP Uptake Studies by Flow Cytometry: One day before performing the experiment, KB cells were seeded in a 24-well plate. Each well contained 60 000 cells dispersed in 1 mL medium. On the next day, the medium was removed and replaced with 400 µL fresh medium. Next, 100 µL functionalized NPs in HBG were added to each well. After 1 h, the medium was removed by aspiration and each well was washed with 1 mL of PBS followed by trypsinization (5 min, 37 °C) with 200 µL of trypsin/EDTA. A total of 400 µL medium was added to each well and the cells were centrifuged (5 min, 1500 rpm, room temperature). In order to have enough cells for analysis, two independent wells per condition were pooled. The supernatant was removed and the cells were resuspended in 700 µL FACS-buffer (10% FBS in PBS) and stored on ice. Directly prior to analysis, 2 µL DAPI (1 mg mL^{-1}) was added to each vial. Data were recorded utilizing the LSR Fortessa flow cytometer (BD Biosciences, Eysins, Switzerland). Gating and data analysis were performed with the FlowJo 7.6.5 flow cytometry analysis software. Initially, cells were gated by forward/sideward scatter and pulse width in order to exclude cell aggregates. Dead cells were subsequently excluded using DAPI and only isolated viable cells were evaluated. Approximately 10 000 gated cells per sample were collected. The

threshold level for NP binding was determined based on the fluorescence of HBG-treated control wells.

Statistical Analysis: If not stated otherwise within the manuscript or respective methods part, data are presented as mean ± standard deviation. Triplicates were analyzed for DLS measurements, ICP–AES, and PMX content by HPLC. For SEM, the as-obtained images were normalized to the scale bar and the size of 100 particles was subsequently analyzed. In flow cytometry experiments, a minimum of 10 000 gated cells were evaluated per condition. For the PMX content determination by HPLC, a PMX calibration curve (six data points between 0 nmol and 5 nmol) was recorded ($R^2 = 0.9976$). MTT experiments were performed in quintuplicates and the data were analyzed by two-way ANOVA utilizing GraphPad Prism version 6.01. Testing was performed with $\alpha = 0.05$ and $n = 5$. After performing the analysis, stars were assigned according to the *p*-values: *for $p \leq 0.05$, **for $p \leq 0.01$, *** for $p \leq 0.001$, and **** for $p \leq 0.0001$.

Supporting Information

Supporting Information is available from the Wiley Online Library or from the author.

Acknowledgements

The authors are grateful for financial support from the Excellence Cluster Nanosystems Initiative Munich (NIM) and the Center for NanoScience, Ludwig-Maximilians-Universität Mnchen. E.W. and M.B. appreciate funding through DFG SFB1066-2. U.L. appreciates support by the Galenus-Privatstiftung (Vienna, Austria). B.S. thanks his family for encouraging scientific curiosity. The authors also thank Dr. Steffen Schmidt for his expertise regarding scanning electron microscopy, Jaroslava Obel for help with ICP–AES, Tina Reuther for assistance with BET and TGA, Wolfgang Rödl and Olga Brück for technical support. The authors are also grateful toward Maike Däther and Johanna Streubel for their assistance during initial exploratory formulation studies. Dr. Philipp Klein, Jasmin Kuhn, and Özgür Öztürk contributed fruitful scientific discussions.

Conflict of Interest

The authors declare no conflict of interest.

Keywords

coordination polymers, drug delivery, metal organic, nanocarriers, receptor targeting

Received: June 28, 2019
Revised: August 28, 2019
Published online: September 24, 2019

[1] a) D. Peer, J. M. Karp, S. Hong, O. C. Farokhzad, R. Margalit, R. Langer, *Nat. Nanotechnol.* **2007**, *2*, 751; b) T. Sun, Y. S. Zhang, B. Pang, D. C. Hyun, M. Yang, Y. Xia, *Angew Chem Int Ed Engl.* **2014**, *53*, 12320.

[2] a) A. M. Rahman, S. W. Yusuf, M. S. Ewer, *Int. J. Nanomed.* **2007**, *2*, 567; b) A. Wicki, D. Witzigmann, V. Balasubramanian, J. Huwyler, *J. Controlled Release* **2015**, *200*, 138.

[3] C. He, K. Lu, D. Liu, W. Lin, *J. Am. Chem. Soc.* **2014**, *136*, 5181.

[4] a) M. E. Davis, Z. G. Chen, D. M. Shin, *Nat. Rev. Drug Discovery* **2008**, *7*, 771; b) J. Jeevanandam, Y. S. Chan, M. K. Danquah, *Biochimie* **2016**, *128–129*, 99.

[5] a) D. Bobo, K. J. Robinson, J. Islam, K. J. Thurecht, S. R. Corrie, *Pharm. Res.* **2016**, *33*, 2373; b) R. Duncan, R. Gaspar, *Mol. Pharmaceutics* **2011**, *8*, 2101.

[6] Y. L. Franco, T. R. Vaidya, S. Ait-Oudhia, *Breast Cancer* **2018**, *10*, 131.

[7] N. V. S. Vallabani, S. Singh, *3 Biotech* **2018**, *8*, 279.

[8] a) M. Eddaoudi, D. B. Moler, H. Li, B. Chen, T. M. Reineke, M. O'Keeffe, O. M. Yaghi, *Acc. Chem. Res.* **2001**, *34*, 319; b) H. Furukawa, K. E. Cordova, M. O'Keeffe, O. M. Yaghi, *Science* **2013**, *341*, 1230444; c) O. M. Yaghi, M. O'Keeffe, N. W. Ockwig, H. K. Chae, M. Eddaoudi, J. Kim, *Nature* **2003**, *423*, 705.

[9] S. Wang, C. M. McGuirk, A. d'Aquino, J. A. Mason, C. A. Mirkin, *Adv. Mater.* **2018**, *30*, 1800202.

[10] P. Z. Moghadam, A. Li, S. B. Wiggin, A. Tao, A. G. P. Maloney, P. A. Wood, S. C. Ward, D. Fairen-Jimenez, *Chem. Mater.* **2017**, *29*, 2618.

[11] S. Kitagawa, R. Kitaura, S. Noro, *Angew. Chem., Int. Ed.* **2004**, *43*, 2334.

[12] N. Stock, S. Biswas, *Chem. Rev.* **2012**, *112*, 933.

[13] S. M. J. Rogge, A. Bavykina, J. Hajek, H. Garcia, A. I. Olivos-Suarez, A. Sepúlveda-Escribano, A. Vimont, G. Clet, P. Bazin, F. Kapteijn, M. Daturi, E. V. Ramos-Fernandez, F. X. Llabrés i Xamena, V. Van Speybroeck, J. Gascon, *Chem. Soc. Rev.* **2017**, *46*, 3134.

[14] Y. He, W. Zhou, G. Qian, B. Chen, *Chem. Soc. Rev.* **2014**, *43*, 5657.

[15] K. Adil, Y. Belmabkhout, R. S. Pillai, A. Cadiau, P. M. Bhatt, A. H. Assen, G. Maurin, M. Eddaoudi, *Chem. Soc. Rev.* **2017**, *46*, 3402.

[16] L. E. Kreno, K. Leong, O. K. Farha, M. Allendorf, R. P. Van Duyne, J. T. Hupp, *Chem. Rev.* **2012**, *112*, 1105.

[17] a) I. Abanades Lazaro, S. Haddad, J. M. Rodrigo-Munoz, R. J. Marshall, B. Sastre, V. Del Pozo, D. Fairen-Jimenez, R. S. Forgan, *ACS Appl. Mater. Interfaces* **2018**, *10*, 31146; b) I. Abanades Lazaro, S. Haddad, S. Sacca, C. Orellana-Tavra, D. Fairen-Jimenez, R. S. Forgan, *Chem.* **2017**, *2*, 561; . c) P. Horcajada, T. Chalati, C. Serre, B. Gillet, C. Sebrie, T. Baati, J. F. Eubank, D. Heurtaux, P. Clayette, C. Kreuz, J. S. Chang, Y. K. Hwang, V. Marsaud, P. N. Bories, L. Cynober, S. Gil, G. Ferey, P. Couvreur, R. Gref, *Nat. Mater.* **2010**, *9*, 172; d) P. Horcajada, R. Gref, T. Baati, P. K. Allan, G. Maurin, P. Couvreur, G. Férey, R. E. Morris, C. Serre, *Chem. Rev.* **2012**, *112*, 1232; e) T. Simon-Yarza, M. Gimenez-Marques, R. Mrimi, A. Mielcarek, R. Gref, P. Horcajada, C. Serre, P. Couvreur, *Angew. Chem., Int. Ed.* **2017**, *56*, 15565; f) K. M. L. Taylor-Pashow, J. Della Rocca, Z. Xie, S. Tran, W. Lin, *J. Am. Chem. Soc.* **2009**, *131*, 14261; g) M.-X. Wu, Y.-W. Yang, *Adv. Mater.* **2017**, *29*, 1606134; h) J. Zhuang, C. H. Kuo, L. Y. Chou, D. Y. Liu, E. Weerapana, C. K. Tsung, *ACS Nano* **2014**, *8*, 2812.

[18] R. Freund, U. Lächelt, T. Gruber, B. Ruhle, S. Wuttke, *ACS Nano* **2018**, *12*, 2094.

[19] a) C. He, C. Poon, C. Chan, S. D. Yamada, W. Lin, *J. Am. Chem. Soc.* **2016**, *138*, 6010; b) W. J. Rieter, K. M. Pott, K. M. Taylor, W. Lin, *J. Am. Chem. Soc.* **2008**, *130*, 11584.

[20] J. G. Heck, C. Feldmann, *J. Colloid Interface Sci.* **2016**, *481*, 69.

[21] R. C. Huxford, K. E. Dekrafft, W. S. Boyle, D. Liu, W. Lin, *Chem Sci.* **2012**, 3.

[22] a) K. Al-Saleh, C. Quinton, P. M. Ellis, *Curr Oncol.* **2012**, *19*, e9; b) P. Tomasini, F. Barlesi, C. Mascaux, L. Greillier, *Ther Adv Med Oncol.* **2016**, *8*, 198.

[23] a) I. Abánades Lázaro, S. Haddad, J. M. Rodrigo-Muñoz, R. J. Marshall, B. Sastre, V. del Pozo, D. Fairen-Jimenez, R. S. Forgan, *ACS Appl. Mater. Interfaces* **2018**, *10*, 31146; b) C. Arcuri, L. Monarca, F. Ragonese, C. Mecca, S. Bruscoli, S. Giovagnoli, R. Donato, O. Bereshchenko, B. Fioretti, F. Costantino, *Nanomaterials* **2018**, 8.

[24] a) M. Kandiah, M. H. Nilsen, S. Usseglio, S. Jakobsen, U. Olsbye, M. Tilset, C. Larabi, E. A. Quadrelli, F. Bonino, K. P. Lillerud, *Chem. Mater.* **2010**, *22*, 6632; b) J. Ren, N. M. Musyoka, H. W. Langmi, T.

Segakweng, B. C. North, M. Mathe, X. Kang, *Int. J. Hydrogen Energy* **2014**, *39*, 12018.
[25] G. Wißmann, A. Schaate, S. Lilienthal, I. Bremer, A. M. Schneider, P. Behrens, *Microporous Mesoporous Mater.* **2012**, *152*, 64.
[26] X. G. Wang, Q. Cheng, Y. Yu, X. Z. Zhang, *Angew. Chem., Int. Ed.* **2018**, *57*, 7836.
[27] E. Blanco, H. Shen, M. Ferrari, *Nat. Biotechnol.* **2015**, *33*, 941.
[28] E. Bagherzadeh, S. M. Zebarjad, H. R. M. Hosseini, *Eur. J. Inorg. Chem.* **2018**, *2018*, 1909.
[29] P. Hirschle, T. Preiß, F. Auras, A. Pick, J. Völkner, D. Valdepérez, G. Witte, W. J. Parak, J. O. Rädler, S. Wuttke, *Cryst Eng Comm.* **2016**, *18*, 4359.
[30] S. Brunauer, P. H. Emmett, E. Teller, *J. Am. Chem. Soc.* **1938**, *60*, 309.
[31] J. G. Heck, J. Napp, S. Simonato, J. Mollmer, M. Lange, H. M. Reichardt, R. Staudt, F. Alves, C. Feldmann, *J. Am. Chem. Soc.* **2015**, *137*, 7329.
[32] a) Y. Kobayashi, H. Katakami, E. Mine, D. Nagao, M. Konno, L. M. Liz-Marzan, *J. Colloid Interface Sci.* **2005**, *283*, 392; b) S. Liu, M. Y. Han, *Chem Asian J.* **2010**, *5*, 36; c) G. Y. Xu, C. H. Zong, Y. A. Sun, X. X. Wang, N. Zhang, F. Wang, A. X. Li, Q. H. Li, *J. Nanosci. Nanotechnol.* **2019**, *19*, 5893.
[33] R. Kishor, A. K. Ghoshal, *RSC Adv.* **2016**, *6*, 898.
[34] W. Stöber, A. Fink, E. Bohn, *J. Colloid Interface Sci.* **1968**, *26*, 62.
[35] C. Graf, D. L. J. Vossen, A. Imhof, A. van Blaaderen, *Langmuir* **2003**, *19*, 6693.
[36] L. M. Liz-Marzán, M. Giersig, P. Mulvaney, *Langmuir* **1996**, *12*, 4329.
[37] N. J. Curtin, A. N. Hughes, *Lancet Oncol.* **2001**, *2*, 298.
[38] a) F. Alexis, E. Pridgen, L. K. Molnar, O. C. Farokhzad, *Mol. Pharmaceutics* **2008**, *5*, 505; b) E. Frohlich, *Int. J. Nanomed.* **2012**, *7*, 5577; c) Y. Y. Khine, M. Callari, H. Lu, M. H. Stenzel, *Macromol. Chem. Phys.* **2016**, *217*, 2302.
[39] A. Zimpel, N. Al Danaf, B. Steinborn, J. Kuhn, M. Höhn, T. Bauer, P. Hirschle, W. Schrimpf, H. Engelke, E. Wagner, M. Barz, D. C. Lamb, U. Lächelt, S. Wuttke, *ACS Nano* **2019**, *13*, 3884. https://doi.org/10.1021/acsnano.8b06287
[40] A. Birke, D. Huesmann, A. Kelsch, M. Weilbacher, J. Xie, M. Bros, T. Bopp, C. Becker, K. Landfester, M. Barz, *Biomacromolecules* **2014**, *15*, 548.
[41] a) A. Birke, J. Ling, M. Barz, *Prog. Polym. Sci.* **2018**, *81*, 163; b) K. Klinker, M. Barz, *Macromol. Rapid Commun.* **2015**, *36*, 1943; c) B. Weber, A. Birke, K. Fischer, M. Schmidt, M. Barz, *Macromolecules* **2018**, *51*, 2653.
[42] D. Finsinger, J. S. Remy, P. Erbacher, C. Koch, C. Plank, *Gene Ther.* **2000**, *7*, 1183.
[43] a) C. He, Y. Hu, L. Yin, C. Tang, C. Yin, *Biomaterials* **2010**, *31*, 3657; b) Y. Yamamoto, Y. Nagasaki, Y. Kato, Y. Sugiyama, K. Kataoka, *J. Controlled Release* **2001**, *77*, 27.
[44] K.-H. Yeon, H. Park, S.-H. Lee, Y.-M. Park, S.-H. Lee, M. Iwamoto, *Korean J. Chem. Eng.* **2008**, *25*, 1040.
[45] C. P. Leamon, P. S. Low, *Proc. Natl. Acad. Sci. USA* **1991**, *88*, 5572.
[46] L. E. Kelemen, *Int. J. Cancer* **2006**, *119*, 243.
[47] J. Sudimack, R. J. Lee, *Adv. Drug Delivery Rev.* **2000**, *41*, 147.
[48] G. L. Zwicke, G. A. Mansoori, C. J. Jeffery, *Nano Reviews* **2012**, *3*. https://doi.org/10.3402/nano.v3i0.18496.
[49] D. M. Loy, P. M. Klein, R. Krzysztoń, U. Lächelt, J. O. Rädler, E. Wagner, *Peer J Preprints* **2019**, *7*, e27669v1.
[50] K. Muller, E. Kessel, P. M. Klein, M. Höhn, E. Wagner, *Mol. Pharmaceutics* **2016**, *13*, 2332.
[51] T. R. Daniels, E. Bernabeu, J. A. Rodriguez, S. Patel, M. Kozman, D. A. Chiappetta, E. Holler, J. Y. Ljubimova, G. Helguera, M. L. Penichet, *Biochim. Biophys. Acta, Gen. Subj.* **2012**, *1820*, 291.
[52] R. Holm, K. Klinker, B. Weber, M. Barz, *Macromol. Rapid Commun.* **2015**, *36*, 2083.
[53] a) O. Schäfer, K. Klinker, L. Braun, D. Huesmann, J. Schultze, K. Koynov, M. Barz, *ACS Macro Lett.* **2017**, *6*, 1140; b) J. Yoo, A. Birke, J. Kim, Y. Jang, S. Y. Song, S. Ryu, B. S. Kim, B. G. Kim, M. Barz, K. Char, *Biomacromolecules* **2018**, *19*, 1602.
[54] M. M. Bradford, *Anal. Biochem.* **1976**, *72*, 248.
[55] E. M. M. Manders, F. J. Verbeek, J. A. Aten, *J Microsc.* **1993**, *169*, 375.